Published on 11 March 2021. Downloaded by University of California - Santa Barbara on 5/15/2021 6:32:38 PM.

NJC

ROYAL SOCIETY OF CHEMISTRY

PAPER

View Article Online
View Journal | View Issue

Cite this: *New J. Chem.*, 2021, **45**, 5509

Two-dimensional van der Waals graphene/transition metal nitride heterostructures as promising high-performance nanodevices

Khang D. Pham,[ab] Cuong Q. Nguyen,*[cd] C. V. Nguyen,[e] Pham V. Cuong[f] and Nguyen V. Hieu*[g]

Received 23rd January 2021,
Accepted 21st February 2021

DOI: 10.1039/d1nj00374g

rsc.li/njc

Graphene-based van der Waals (vdW) heterostructures have attracted much attention because they can enhance the properties of separated materials, possess numerous new phenomena and unusual properties and improve the performance of devices. Motivated by the successful fabrication of single-layer transition metal nitrides (TMNs) [*Science*, 2020, **369**, 670], we investigate the interfacial properties of heterostructures formed by stacking graphene (GR) on two different TMN monolayers, $MoGe_2N_4$ (MGN) and $MoSi_2N_4$ (MSN). Both the GR/MGN and GR/MSN heterostructures are characterized by weak vdW interactions, which preserve the intrinsic electronic properties of both the GR and TMN monolayers. The GR/MGN heterostructure forms an n-type Schottky contact, while a p-type Schottky contact is formed at the GR/MSN interface. Both the barrier and contact types in the GR/MGN heterostructure are sensitive to the electric gating and interlayer coupling. The transformation from an n-type Schottky contact to a p-type one or to an n-type ohmic contact can be achieved in the GR/MGN heterostructure by applying electric gating. In addition, adjusting the interlayer spacings between the GR and MGN layers leads to a transition from n-type to p-type Schottky contact. Our findings demonstrate that the GR/TMN heterostructures can be considered as promising high-performance nanodevices.

1 Introduction

Graphene (GR)[1] and other two-dimensional (2D) materials[2–9] have attracted considerable interest from the research community owing to their intriguing properties and wide range of applications. For instance, an ultrahigh carrier mobility of graphene[10] makes graphene an excellent candidate for nano-electronic devices, such as field effect transistors[11,12] and ultrafast photodetectors.[13] The strong spin–orbit coupling in layered transition metal dichalcogenides[14,15] makes them suitable for spintronics applications. However, despite their advantages, most of these 2D materials have some drawbacks that may limit their applications in many high speed nanodevices. For example, the absence of a sizable band gap in graphene has narrowed its applications in FETs.[11] Therefore, opening a band gap in graphene is one of the most interesting topics in recent years. Nowadays, there are a lot of methods that can be demonstrated for band gap opening in graphene, including doping,[16] functionalization[17] and creating heterostructures.[18–22] Among these, constructing heterostructures by stacking graphene on the surface of various 2D materials is a powerful strategy to improve the performance of the graphene-based devices.[23–26] For instance, Sun *et al.*[27] investigated theoretically the combination between graphene and blue phosphorene. They showed that graphene/blue phosphorene possesses a Schottky contact, which can be tuned by applying an electric field. In addition, the electronic properties of graphene/GaN heterostructures have also been investigated using density functional theory.[28] The transition from n-type to p-type Schottky contact in graphene/GaN heterostructures makes them suitable for the design of Schottky devices. Wang *et al.*[29] predicted that the graphene/GeC heterostructure forms a p-type Schottky contact. Also, this contact can be tuned into an ohmic contact by changing the interlayer coupling. All these

[a] Laboratory of Applied Physics, Advanced Institute of Materials Science, Ton Duc Thang University, Ho Chi Minh City, Vietnam. E-mail: phamdinhkhang@tdtu.edu.vn
[b] Faculty of Applied Sciences, Ton Duc Thang University, Ho Chi Minh City, Vietnam
[c] Institute of Research and Development, Duy Tan University, Da Nang 550000, Vietnam. E-mail: nguyenquangcuong3@duytan.edu.vn
[d] Faculty of Natural Sciences, Duy Tan University, Da Nang 550000, Vietnam
[e] Department of Materials Science and Engineering, Le Quy Don Technical University, Ha Noi 100000, Vietnam. E-mail: chuong.vnguyen@lqdtu.edu.vn
[f] Faculty of Electrical Engineering Technology, Hanoi University of Industry, Hanoi 100000, Vietnam
[g] Faculty of Physics, The University of Danang, University of Science and Education, Da Nang, Vietnam. E-mail: nvhieu@ued.udn.vn

This journal is © The Royal Society of Chemistry and the Centre National de la Recherche Scientifique 2021

Published on 11 March 2021. Downloaded by University of California - Santa Barbara on 5/15/2021 6:32:38 PM.

results indicate that the graphene-based heterostructures are a promising candidate for the design of future nanodevices. In addition, it should be mentioned that graphene-based vdW heterostructures can also be synthesized experimentally by different common strategies, including the transfer method,[30,31] chemical vapor deposition[32] or molecular beam epitaxy.[18]

Recently, a new kind of 2D material, transition metal nitride (TMN), has received more tremendous attention from the scientific community.[33,34] Very recently, Hong *et al.*[35] successfully realized a novel 2D $MoSi_2N_4$ (MSN) high-quality monolayer using a chemical vapor deposition (CVD) approach. The atomic structure of monolayer MSN is composed of a MoN_2 monolayer sandwiched by two Si–N bilayers. Furthermore, Mortazavi and co-workers[34] performed first-principles calculations of the stability and electronic properties of MA_2N_4, where M stands for a transition metal, and A represents the Si or Ge atoms. They showed that all these TMN monolayers can be used for designing and fabricating optoelectronic and photocatalytic nanodevices owing to their appropriate band edge positions and strong visible light absorption. Following these intrinsic properties of TMN monolayers, we will focus on the structural and electronic properties of vdW heterostructures, formed by combining GR and TMN monolayers. Our results demonstrate that the GR/MGN heterostructure forms an n-type Schottky contact with a barrier of 0.63 eV, while a p-type Schottky contact with a barrier of 0.96 eV is formed at the GR/MSN interface. This implies that the GR/MGN heterostructure-based nanodevices can provide better performance than the GR/MSN heterostructure-based devices. The barrier and contact types in the GR/MGN heterostructure are known to be very sensitive to the electric gating and interlayer coupling. Our findings could provide helpful guidance for the design and fabrication of next-generation electronic devices based on GR/TMN heterostructures.

2 Computational methods

All calculations in this work are performed through density functional theory (DFT), which is implemented in the simulated Quantum Espresso package.[36,37] The Perdew–Burke–Ernzerhof (PBE) functional in the framework of the generalized gradient approximation (GGA[38]) is used to describe the correlation–exchange energy. Whereas, the projected augmented wave (PAW) pseudopotentials[39] are adopted to describe the ion–electron bonding. The energy cutoff is calculated to be 500 eV for all calculations, which were fully optimized. The convergence for force and energy are chosen to be 10^{-3} eV Å^{-1} and 10^{-6} eV, respectively. The Brillouin zone (BZ) integration is sampled

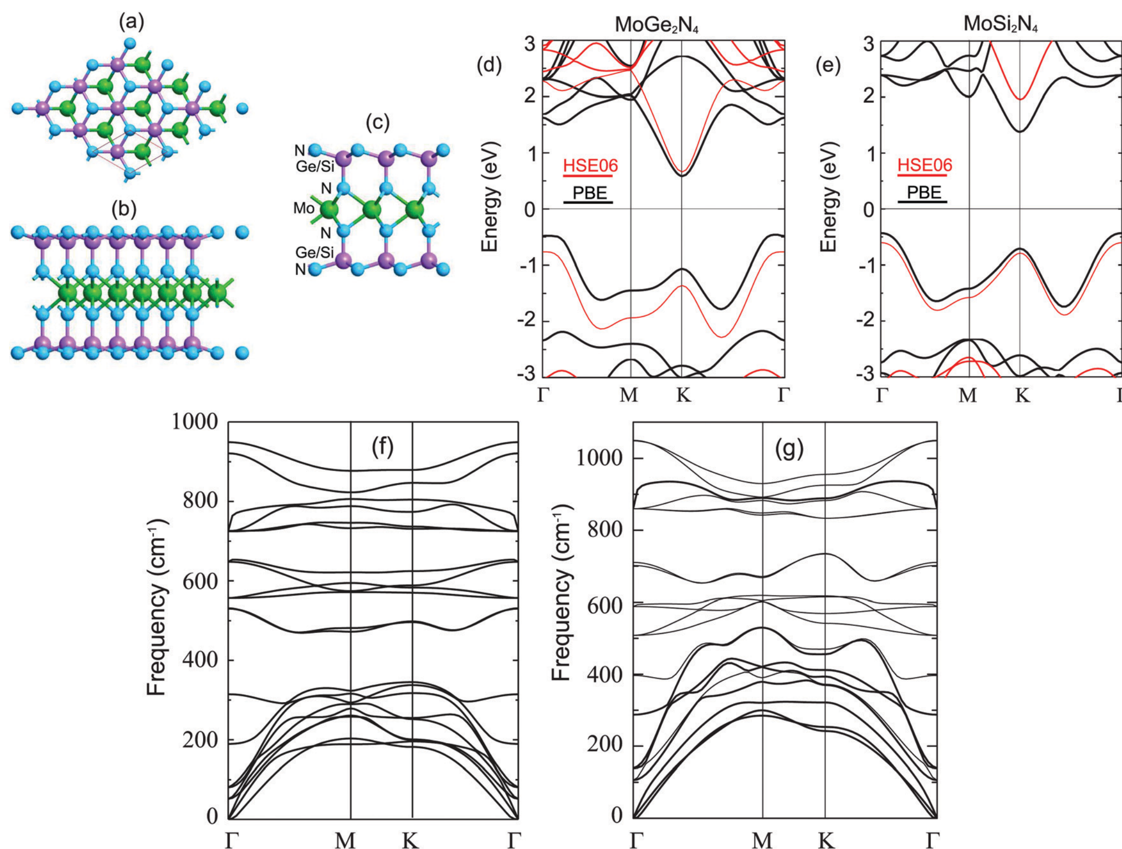

Fig. 1 (a–c) Top, side and front views of the relaxed atomic structure of MoA_2N_4 (A = Ge, Si) monolayers. The band structures of (d) MGN and (e) MSN monolayers calculated by the PBE and HSE06 methods. The Fermi level is set to be zero. The phonon dispersion curves of (f) $MoGe_2N_4$ and (g) $MoSi_2N_4$ monolayers.

This journal is © The Royal Society of Chemistry and the Centre National de la Recherche Scientifique 2021

Published on 11 March 2021. Downloaded by University of California - Santa Barbara on 5/15/2021 6:32:38 PM.

within a 9 × 9 × 1 *k*-point mesh. For avoiding the bonding between the periodic sublayers, we set a large vacuum thickness of 25 Å. The Heyd–Scuseria–Ernzerhof hybrid functional (HSE06) is also used to obtain more accurate value of the band gap. The weak vdW bondings in heterostructures are described by adding the vdW dispersion in DFT-D3 approximation.[40] Dipole correction was applied in all the calculations.

3 Results and discussion

The atomic structure of MoA_2N_4 (A = Ge, Si) monolayers is illustrated in Fig. 1(a–c). One can observe that both the $MoGe_2N_4$ (MGN) and $MoSi_2N_4$ (MSN) monolayers have the same space group of *P*6*m*1 with a hexagonal crystal. The crystal of MoA_2N_4 monolayers is composed of a MoN_2 monolayer sandwiched by two buckled A–N bilayers. This indicates that the MoA_2N_4 monolayers consist of 7 layers, including 4N layers, 2Si layers and 1Mo layer. The thickness of the MoA_2N_4 monolayer is 10.60 Å in the case of A = Ge and 10.12 Å with A = Si. The optimized lattice parameters of the MGN and MSN monolayers are 3.01 Å and 2.90 Å, respectively. These values are in good agreement with the previous reports.[34] Both the MGN and MSN monolayers possess indirect semiconductors. The calculated band gaps of MGN and MSN are 1.03/1.42 eV and 1.81/2.38 eV, respectively, obtained from the PBE/HSE06 method. One can observe that the indirect band gaps of the MGN and MSN monolayers are formed by the valence band maximum (VBM) at the Γ point and the conduction band minimum (CBM) at the K point. Furthermore, both the PBE and HSE06 methods predict the same trend in the band structures of the considered monolayers expect for the band gap values. In addition, we find that the band gap value of the MSN monolayer calculated by the PBE method is closer to the experimental report of 1.94 eV.[35] Therefore, we further perform all the next calculations using the PBE method. The calculated phonon dispersion curves of both these monolayers shown in Fig. 1(f) and (g) confirm their dynamic stability owing to the lack of negative frequencies at the Γ point.

We now construct the atomic structure of vdW heterostructures between GR and MGN (MSN) monolayers. Due to the difference in the lattice parameters between GR and MGN (MSN) monolayers, we use a supercell, which consists of a (2 × 2) GR and a ($\sqrt{3}$ × $\sqrt{3}$) MGN (MSN). The optimized lattice parameters of GR/MGN and GR/MSN heterostructures are 4.97 Å and 4.87 Å, respectively. This indicates that the lattice mismatch in the GR/MGN and GR/MSN heterostructures is 1.80% and 1.65%, respectively. The top and side views of the optimized atomic structures of GR/MGN and GR/MSN are illustrated in Fig. 2. In this stacking configuration, one nitrogen atom in the MSN layer is located directly below the center of the GR hexagonal ring and another nitrogen atom is placed directly below the carbon atom. After the geometric optimization, the

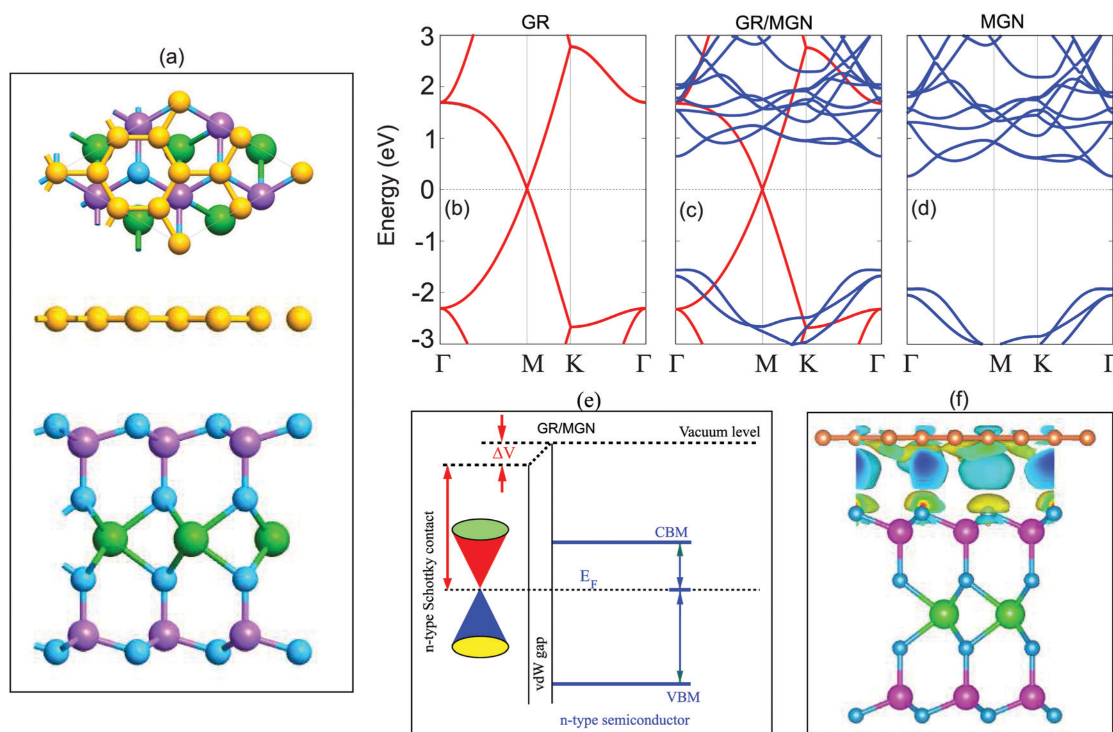

Fig. 2 (a) Top and side views of the optimized atomic structure of GR/MGN (GRM/MSN). Yellow balls represent the carbon atom. Cyan, violet and green balls stand for the nitrogen, silicon and molybdenum atoms, respectively. The projected band structures of (b) isolated GR, (c) the GR/MGN heterostructure and (d) an isolated MGN monolayer. (e) The band diagram and (f) the charge density difference of the GR/MGN heterostructure. The yellow and cyan regions represent the charge accumulation and depletion, respectively. The isosurface of the charge density difference is set to be 3×10^{-4} e Å^{-3}.

Published on 11 March 2021. Downloaded by University of California - Santa Barbara on 5/15/2021 6:32:38 PM.

interlayer spacing between the GR and the topmost nitrogen layer is obtained, which is 3.38 Å for GR/MGN and 3.16 Å for GR/MSN.

We now investigate the electronic properties of both the GR/MGN and GR/MSN heterostructures, as depicted in Fig. 2 and 3, respectively. The projected band structures of isolated (2 × 2) GR, GR/MGN and isolated ($\sqrt{3} \times \sqrt{3}$) MSN are displayed in Fig. 2(b–d). The isolated GR preserves the dispersion Dirac cone around the Fermi level. However, this cone is shifted from the K point in perfect graphene into the M point in its supercell form owing to the band folding effect.[41] This effect was also observed in other graphene-based heterostructures.[42,43] In addition, the isolated MGN and MSN monolayers exhibit n-type and p-type doping semiconductors, as illustrated in Fig. 2(d) and 3(c), resspectively. The strained MGN and MSN monolayers are direct semiconductors with the size of the band gaps of 2.16 eV and 2.45 eV, respectively. The electronic band structures of GR/MGN and GR/MSN are displayed in Fig. 2(c) and 3(b), respectively. The electronic band structures of GR, MGN and MSN monolayers are well preserved in their combined heterostructures. This finding shows that the combined GR/MGN and GR/MSN heterostructures can have the intrinsic properties of monolayers.

In order to confirm the structural stability of such heterostructures, we further establish the binding energy as follows:

$$E_b = \frac{E_{vdWH} - E_{GR} - E_{MGN/MSN}}{N} \quad (1)$$

here, E_{vdWH} is the total energy of the combined GR/MGN or GR/MSN heterostructure. E_{GR}, E_{MGN} and E_{MSN} are the total energy of isolated GR, MGN and MSN monolayers, respectively. N = 8 stands for the number of carbon atoms in the calculated supercell of the heterostructures. The binding energy of the GR/MGN and GR/MSN heterostructures is calculated to be −49.14 meV per C atom and −24.86 meV per C atom, respectively. One can find that these values are comparable with those in other graphene/2D heterostructures,[44] which are typical weak vdW interactions. This indicates that both the GR/MGN and GR/MSN heterostructures are mainly characterized by the weak vdW interactions rather than chemical bonding. The weak vdW interactions in the GR/TMN heterostructures result in the formation of the weak Fermi level pining at the interfaces.

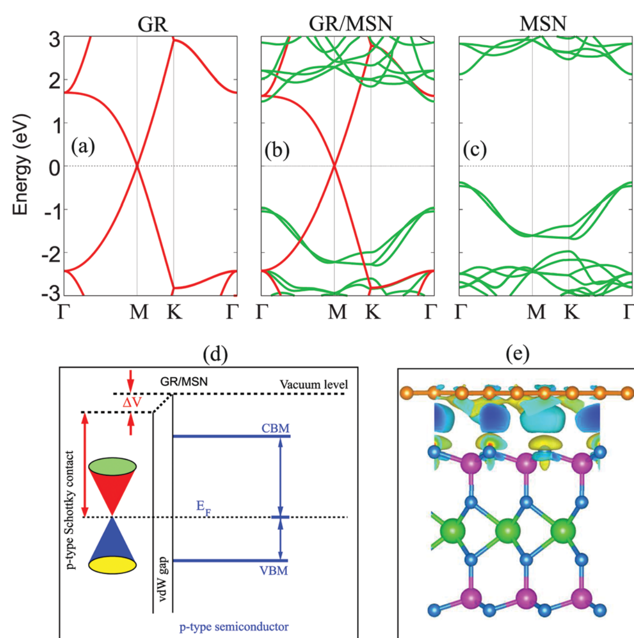

Fig. 3 The projected band structures of (a) isolated GR, (b) the GR/MSN heterostructure and (c) an isolated MSN monolayer. (d) The band diagram and (e) the charge density difference of the GR/MSN heterostructure. The yellow and cyan regions represent the charge accumulation and depletion, respectively. The isosurface of the charge density difference is set to be 3 × 10^{-4} e Å^{-3}.

More interestingly, when the contact of GR/MGN and GR/MSN is formed, it tends to the formation of the Schottky or ohmic contact at the interface. One can observe from the projected band structures of GR/MGN (see Fig. 2(c)) and GR/MSN (see Fig. 3(b)) that the Fermi level of the GR layer lies between the VB and CB of semiconducting MGN and MSN layers, resulting in the formation of a Schottky contact in both the GR/MGN and GR/MSN heterojunctions. Due to the weak vdW interactions, the Schottky contact in such heterostructures is characterized by the Schottky barrier of n-type and p-type, which can be established by the Schottky–Mott rule[45] as follows: $\Phi_n = E_{CB} - E_F$ and $\Phi_p = E_F - E_{VB}$. The band diagrams of the GR/MGN and GR/MSN heterostructures are displayed in Fig. 2(e) and 3(d), respectively. The calculated Φ_n and Φ_p for the GR/MGN heterostructure are 0.63 eV and 1.54 eV, respectively, while they respectively are 1.49 eV and 0.96 eV for the GR/MSN heterostructure. This demonstrates that the GR/MGN forms the n-type Schottky contact because the Φ_n barrier is smaller than that of Φ_p, while the GR/MSN heterostructure forms the p-type Schottky contact with the Φ_n barrier enlarged compared to the Φ_p. In addition, one can find that the Schottky barrier at the GR/MGN interface is smaller than that at the GR/MSN interface, demonstrating that GR/MGN heterostructure-based nanodevices can provide better performance than the GR/MSN heterostructure-based devices.

Furthermore, to understand the charge transfer mechanism in these heterostructures, we calculate the charge density difference as: $\Delta\rho = \rho_{vdWH} - \rho_{GR} - \rho_{MGN/MSN}$, where ρ_{vdWH}, ρ_{GR}, and $\rho_{MGN/MSN}$, respectively, are the total energy of the GR/MGN or GR/MSN heterostructure, isolated GR and MGN/MSN monolayers. The yellow and cyan regions represent the electron gain and loss, respectively, as illustrated in Fig. 2(f) and 3(e). This demonstrates that the charges are accumulated in the MGN and MSN layers, whereas they are depleted in the GR layer. The Bader charge analysis demonstrates that there are only 0.003 e transferred from the GR layer to the MGN and MSN layers.

Furthermore, we investigate the ability to modify the Schottky barrier and contact in the heterojunction formed between GR and MGN or MSN monolayer by adjusting the interlayer coupling or applying electrical gating. Due to the lower Schottky barrier of the GR/MGN heterostructure compared to GR/MGN, we further focused on the GR/MGN heterostructure. We believe

This journal is © The Royal Society of Chemistry and the Centre National de la Recherche Scientifique 2021

Published on 11 March 2021. Downloaded by University of California - Santa Barbara on 5/15/2021 6:32:38 PM.

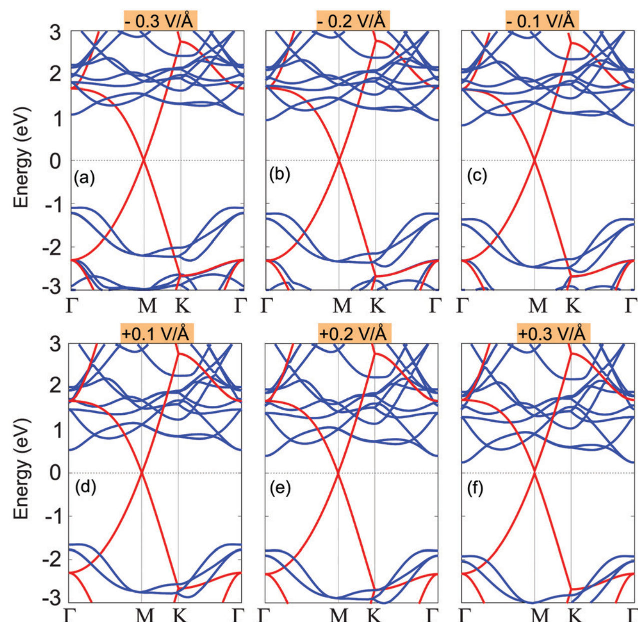

Fig. 4 The projected band structure of the GR/MGN heterostructure under different strengths of electric field, ranging from (a) -0.3 V Å^{-1}, to (b) -0.2 V Å^{-1}, (c) -0.1 V Å^{-1}, (d) +0.1 V Å^{-1}, (e) +0.2 V Å^{-1} and (f) +0.3 V Å^{-1}. The Fermi level is set to zero. The red and blue lines represent the contributions of the GR and MGN layers, respectively.

that the same trend will occur in the GR/MSN heterostructure. The electronic structures of GR/MGN heterostructures under different strengths of electric gating are depicted in Fig. 4. The electric gating is applied along the z direction of the heterostructure with the range from -0.3 V Å^{-1} to +0.3 VÅ. From Fig. 4(a–c), we observe that applying negative electric gating leads to the shift in the Fermi level of graphene from the CB to VB of the semiconducting MGN layer. This implies that the negative electric gating tends to an increase in the n-type barrier, whereas the p-type barrier has decreased accordingly. The linear variation in the Schottky barrier of the GR/MGN heterostructure is depicted in Fig. 5(a). Due to such linear change of the Schottky barrier, the n-type barrier is larger than the p-type one when the electric gating is more negative than -0.3 V Å^{-1}. This indicates that the transformation from n-type to p-type Schottky contact can be achieved at the GR/MGN interface when the negative gating is applied. Consequently, the Fermi level of graphene is shifted upwards from the VB to the CB of the semiconducting MGN layer if the positive gating is used, as depicted in Fig. 4(d–f). This implies that the positive gating tends to a decrease in the n-type barrier, while the p-type barrier increases accordingly, as depicted in Fig. 5(a). Following the linear decrease in the n-type barrier, we can find that such a barrier can reach a zero or negative value when the gating is more positive than +0.46 V Å^{-1}. This finding shows that the n-type Schottky contact in GR/MGN can transform into an n-type ohmic contact when the positive electric gating of +0.46 V Å^{-1} is applied. Therefore, we can conclude that both the Schottky barrier and contact types of the GR/MGN heterostructure are very sensitive to the external electric gating with the transformation from n-type Schottky contact to the p-type one or to n-type ohmic contact.

Next, we consider the effect of interlayer spacing on the contact barriers and types of GR/MGN heterostructure. The variation of the Schottky barrier of the GR/MGN heterostructure as a function of interlayer spacing is depicted in Fig. 5(b). We find that with decreasing the interlayer spacings from 4.28 Å to 2.78 Å, the Φ_n increases from 0.33 eV to 1.16 eV, respectively, while the Φ_p decreases accordingly from 1.85 eV to 0.94 eV. It should be noted that the binding energy of the GR/MGN heterostructure at the interlayer spacing of 4.28 Å is calculated to be -13.75 meV per C atom, confirming the structural stability of such heterostructure. Interestingly, we find from Fig. 5(b) that when the interlayer spacing is shorter than 2.8 Å, the Φ_p is shorter than the Φ_n, indicating the transformation from an n-type Schottky contact to a p-type one in the GR/MGN heterostructure. The projected band structures of the GR/MGN heterostructure under different interlayer spacings are depicted in Fig. 6. With increasing interlayer

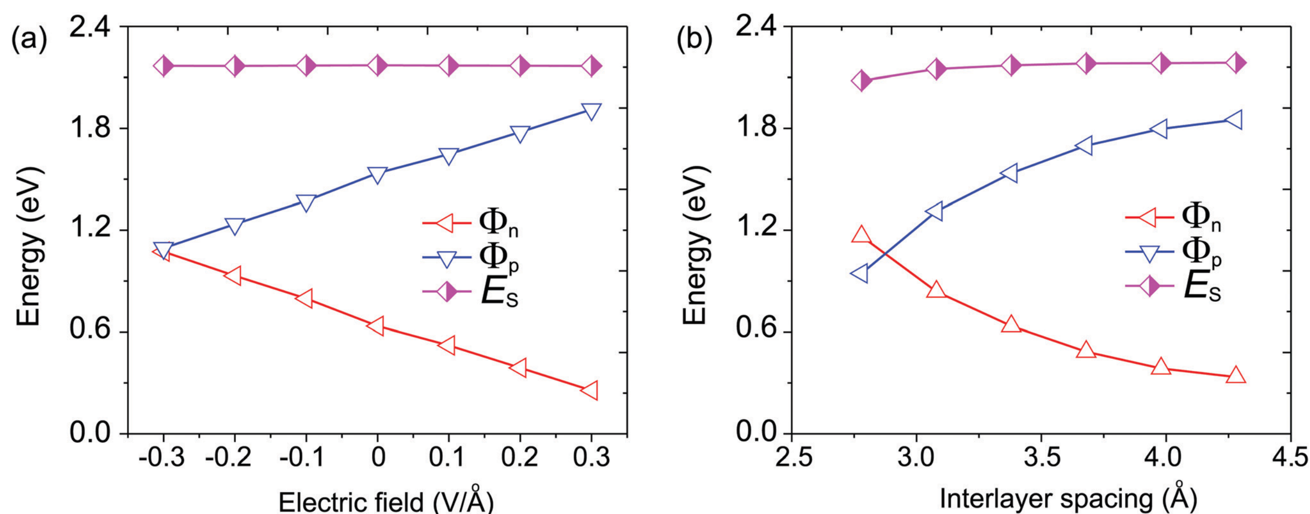

Fig. 5 The variations of the n-type and p-type barriers of the GR/MGN heterostructure as a function of (a) electric field and (b) interlayer spacing.

Published on 11 March 2021. Downloaded by University of California - Santa Barbara on 5/15/2021 6:32:38 PM.

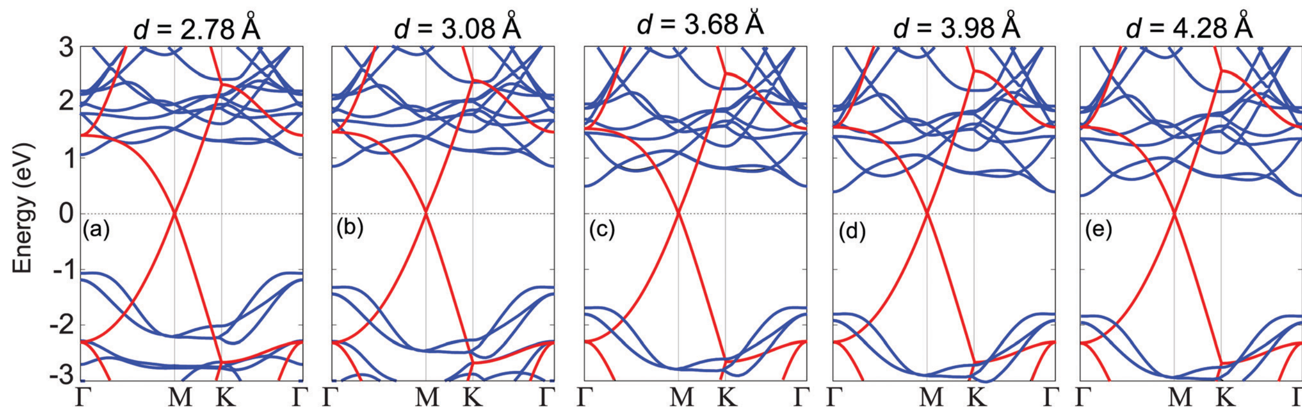

Fig. 6 The projected band structures of the GR/MGN heterostructure under different interlayer spacings of (a) 2.78 Å, (b) 3.08 Å, (c) 3.68 Å, (d) 3.98 Å and (e) 4.28 Å. Red and blue lines represent the contributions of GR and MGN layers in their GR/MGN heterostructure.

spacing, the Fermi level of the GR layer moves upwards from the VB to the CB of the semiconducting MGN layer. In this way, the Φ_n increases with the increasing interlayer spacing, whereas the Φ_n decreases accordingly. At the interlayer spacing of 2.78 Å the Fermi level of the GR layer is closer to the CB than the VB of the MGN layer, demonstrating the the GR/MGN heterostructure forms a p-type Schottky contact. Therefore, by adjusting the interlayer spacing between the GR and MGN layers in the GR/MGN heterostructure, the transformation from n-type to p-type Schottky contact can be achieved. It should be noted that the underlying mechanism for the transition for the transition from n-type to p-type Schottky contact or to ohmic contact under electric field and strain engineering can be established by analyzing the charge transfers between GR and MGN layers. For instance, when the interlayer spacing is decreased, the interactions between the GR and MGN layers are strengthened.

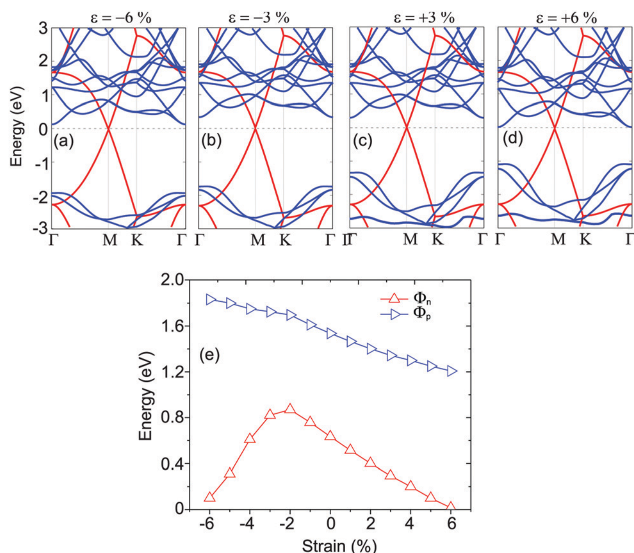

Fig. 7 The projected band structures of the GR/MGN heterostructure under different in-plane biaxial strains of (a) −6%, (b) −3%, (c) +3% and (d) +6%. (e) The evaluation of the Schottky barrier of the GR/MGN heterostructure as a function of in-plane biaxial strain.

Thus, more electrons will transfer from the GR layer to the MGN layer. This transportation leads to the shift of the GR's Fermi level closer to the VBM of the MGN layer, thus leading to the transition from an n-type Schottky contact to a p-type one.

The effect of in-plane biaxial strain on the contact barrier and contact type of the GR/MGN heterostructure was also investigated. One can observe from Fig. 7 that the electronic properties, including the Schottky barriers and contact types of the GR/MGN heterostructure are significantly changed under biaxial strains. The p-type barrier of the GR/MGN heterostructure is decreased with the strain range of −6% to 6%. Whereas, the n-type barrier of the GR/MGN heterostructure is increased when the compressive biaxial strain is smaller than −2%. This barrier is continuously decreased when the large compressive strain is applied. On the other hand, the tensile biaxial strain leads to a decrease in the n-type Schottky contact. When the tensile strain reaches +6%, the n-type Schottky barrier reaches 0 eV, implying that the GR/MGN heterostructure transforms from an n-type Schottky contact to an n-type ohmic contact. The above results show that both the contact barriers and contact types of the GR/MGN heterostructure can be controlled by applying in-plane biaxial strains.

4 Conclusions

We have investigated systematically the electronic properties of heterostructures formed between GR and transition metal nitrides, including $MoGe_2N_4$ and $MoSi_2N_4$ monolayers. The weak vdW interactions in the GR/TMN heterostructures preserve the intrinsic electronic properties of both the GR and TMN monolayers. We found that the GR/MGN heterostructure forms an n-type Schottky contact with a barrier of 0.63 eV, while a p-type Schottky contact with a barrier of 0.96 eV is formed at the GR/MSN interface. Both these heterostructures are structurally stable, and thus, they can be fabricated easily in a recent experiment. The barrier and contact types in the GR/MGN heterostructure are known to be very sensitive to the external conditions, including external electric gating and interlayer coupling. The transformation from an n-type Schottky contact

This journal is © The Royal Society of Chemistry and the Centre National de la Recherche Scientifique 2021

View Article Online

Published on 11 March 2021. Downloaded by University of California - Santa Barbara on 5/15/2021 6:32:38 PM.

to a p-type one or to an n-type ohmic contact can be achieved in the GR/MGN heterostructure under applying electric gating. In addition, adjusting the interlayer spacings between the GR and MGN layers leads to a transition from n-type to p-type Schottky contact. Our findings could provide helpful guidance for the design and fabrication of next-generation electronic devices based on GR/TMN heterostructures.

Conflicts of interest

There are no conflicts to declare.

Acknowledgements

This research was funded by Vietnam National Foundation for Science and Technology Development (NAFOSTED) under grant number 103.01-2019.05.

References

1 K. S. Novoselov, A. K. Geim, S. V. Morozov, D. Jiang, Y. Zhang, S. V. Dubonos, I. V. Grigorieva and A. A. Firsov, *Science*, 2004, **306**, 666.
2 M. Sun and U. Schwingenschlögl, *Phys. Rev. Appl.*, 2020, **14**, 044015.
3 Q. H. Wang, K. Kalantar-Zadeh, A. Kis, J. N. Coleman and M. S. Strano, *Nat. Nanotechnol.*, 2012, **7**, 699.
4 S. Wang, M. S. Ukhtary and R. Saito, *Phys. Rev. Res.*, 2020, **2**, 033340.
5 S. Manzeli, D. Ovchinnikov, D. Pasquier, O. V. Yazyev and A. Kis, *Nat. Rev. Mater.*, 2017, **2**, 17033.
6 M. Sun, Y. Yan and U. Schwingenschlòĝl, *J. Phys. Chem. Lett.*, 2020, **11**, 9051.
7 Z. Guan and S. Ni, *ACS Appl. Mater. Interfaces*, 2020, **12**, 53067.
8 S. Balendhran, S. Walia, H. Nili, S. Sriram and M. Bhaskaran, *Small*, 2015, **11**, 640.
9 A. Carvalho, M. Wang, X. Zhu, A. S. Rodin, H. Su and A. H. C. Neto, *Nat. Rev. Mater.*, 2016, **1**, 1.
10 K. I. Bolotin, K. J. Sikes, Z. Jiang, M. Klima, G. Fudenberg, J. E. Hone, P. Kim and H. Stormer, *Solid State Commun.*, 2008, **146**, 351.
11 F. Xia, D. B. Farmer, Y.-M. Lin and P. Avouris, *Nano Lett.*, 2010, **10**, 715.
12 L. Vicarelli, M. Vitiello, D. Coquillat, A. Lombardo, A. C. Ferrari, W. Knap, M. Polini, V. Pellegrini and A. Tredicucci, *Nat. Mater.*, 2012, **11**, 865.
13 F. Xia, T. Mueller, Y.-M. Lin, A. Valdes-Garcia and P. Avouris, *Nat. Nanotechnol.*, 2009, **4**, 839.
14 X. Xu, W. Yao, D. Xiao and T. F. Heinz, *Nat. Phys.*, 2014, **10**, 343.
15 Z. Y. Zhu, Y. C. Cheng and U. Schwingenschlögl, *Phys. Rev. B*, 2011, **84**, 153402.
16 T. Wehling, K. Novoselov, S. Morozov, E. Vdovin, M. Katsnelson, A. Geim and A. Lichtenstein, *Nano Lett.*, 2008, **8**, 173.
17 T. Kuila, S. Bose, A. K. Mishra, P. Khanra, N. H. Kim and J. H. Lee, *Prog. Mater. Sci.*, 2012, **57**, 1061.
18 Z. Ben Aziza, H. Henck, D. Pierucci, M. G. Silly, E. Lhuillier, G. Patriarche, F. Sirotti, M. Eddrief and A. Ouerghi, *ACS Nano*, 2016, **10**, 9679.
19 B. Zhou, X. Wang, S. Dong, K. Zhang and W. Mi, *Carbon*, 2017, **120**, 121.
20 W. Guo, X. Ge, S. Sun, Y. Xie and X. Ye, *Phys. Chem. Chem. Phys.*, 2020, **22**, 4946.
21 A. Nourbakhsh, A. Zubair, M. S. Dresselhaus and T. Palacios, *Nano Lett.*, 2016, **16**, 1359.
22 F. Ceballos, M. Z. Bellus, H.-Y. Chiu and H. Zhao, *Nanoscale*, 2015, **7**, 17523.
23 P. Sols-Fernández, M. Bissett and H. Ago, *Chem. Soc. Rev.*, 2017, **46**, 4572.
24 J. Tan, A. Avsar, J. Balakrishnan, G. Koon, T. Taychatanapat, E. O'Farrell, K. Watanabe, T. Taniguchi, G. Eda and A. Castro Neto, *et al.*, *Appl. Phys. Lett.*, 2014, **104**, 183504.
25 I. Lee, W. T. Kang, Y. S. Shin, Y. R. Kim, U. Y. Won, K. Kim, D. L. Duong, K. Lee, J. Heo and Y. H. Lee, *et al.*, *ACS Nano*, 2019, **13**, 8392.
26 M. Sun, J.-P. Chou, J. Yu and W. Tang, *J. Mater. Chem. C*, 2017, **5**, 10383.
27 M. Sun, J.-P. Chou, J. Yu and W. Tang, *Phys. Chem. Chem. Phys.*, 2017, **19**, 17324.
28 M. Sun, J.-P. Chou, Q. Ren, Y. Zhao, J. Yu and W. Tang, *Appl. Phys. Lett.*, 2017, **110**, 173105.
29 S. Wang, J.-P. Chou, C. Ren, H. Tian, J. Yu, C. Sun, Y. Xu and M. Sun, *Sci. Rep.*, 2019, **9**, 1.
30 H. Henck, Z. B. Aziza, D. Pierucci, F. Laourine, F. Reale, P. Palczynski, J. Chaste, M. G. Silly, F. Bertran and P. Le Fèvre, *et al.*, *Phys. Rev. B*, 2018, **97**, 155421.
31 D. Pierucci, H. Henck, J. Avila, A. Balan, C. H. Naylor, G. Patriarche, Y. J. Dappe, M. G. Silly, F. Sirotti and A. C. Johnson, *et al.*, *Nano Lett.*, 2016, **16**, 4054.
32 S. K. Chong, F. Long, G. Wang, Y.-C. Lin, S. Bhandari, R. Shahbazian-Yassar, K. Suenaga, R. Pandey and Y. K. Yap, *ACS Appl. Nano Mater.*, 2018, **1**, 3293.
33 R. Ningthoujam and N. Gajbhiye, *Prog. Mater. Sci.*, 2015, **70**, 50.
34 B. Mortazavi, B. Javvaji, F. Shojaei, T. Rabczuk, A. V. Shapeev and X. Zhuang, *Nano Energy*, 2020, **82**, 105716.
35 Y.-L. Hong, Z. Liu, L. Wang, T. Zhou, W. Ma, C. Xu, S. Feng, L. Chen, M.-L. Chen and D.-M. Sun, *et al.*, *Science*, 2020, **369**, 670.
36 P. Giannozzi, S. Baroni, N. Bonini, M. Calandra, R. Car, C. Cavazzoni, D. Ceresoli, G. L. Chiarotti, M. Cococcioni and I. Dabo, *et al.*, *J. Phys.: Condens. Matter*, 2009, **21**, 395502.
37 P. Giannozzi, O. Andreussi, T. Brumme, O. Bunau, M. B. Nardelli, M. Calandra, R. Car, C. Cavazzoni, D. Ceresoli and M. Cococcioni, *et al.*, *J. Phys.: Condens. Matter*, 2017, **29**, 465901.
38 J. P. Perdew, K. Burke and M. Ernzerhof, *Phys. Rev. Lett.*, 1996, **77**, 3865.
39 G. Kresse and D. Joubert, *Phys. Rev. B: Condens. Matter Mater. Phys.*, 1999, **59**, 1758.
40 S. Grimme, *J. Comput. Chem.*, 2006, **27**, 1787.

41 Y.-C. Zhou, H.-L. Zhang and W.-Q. Deng, *Nanotechnology*, 2013, **24**, 225705.
42 Y. Li, J. Wang, B. Zhou, F. Wang, Y. Miao, J. Wei, B. Zhang and K. Zhang, *Phys. Chem. Chem. Phys.*, 2018, **20**, 24109.
43 Z. Guan, S. Ni and S. Hu, *RSC Adv.*, 2017, **7**, 45393.
44 J. Padilha, A. Fazzio and A. J. da Silva, *Phys. Rev. Lett.*, 2015, **114**, 066803.
45 J. Bardeen, *Phys. Rev.*, 1947, **71**, 717.

Published on 11 March 2021. Downloaded by University of California - Santa Barbara on 5/15/2021 6:32:38 PM.

This journal is © The Royal Society of Chemistry and the Centre National de la Recherche Scientifique 2021